



Comparison of Predicted and Measured Performance of a Large Cavern in the Himalayas

R. K. BHASIN†
N. BARTON†
E. GRIMSTAD†
P. CHRYSSANTHAKIS†
F. P. SHENDE‡

Detailed investigative and performance monitoring studies have been carried out at the site of an underground powerhouse cavern in the Himalayan Region of India. The updated empirical (Q-system) and numerical (UDEC-BB) approaches, applied for predicting the behaviour of the rock mass prior to the construction of the underground cavern (20 × 49 × 216 m), have been compared with the instrumentation data from multi point borehole extensometers (MPBX). Upon completion of the first numerical excavation step (20 m span arch), a relatively high stress-strength ratio and a maximum deformation of approx. 18 mm was predicted in the roof of the cavern. MPBX readings in the arch have indicated maximum deformations in the range 19–24 mm with the 20 m span fully excavated. The results of numerically excavating the cavern to its full height (49 m), have indicated maximum deformations in the range 43–45 mm in the walls of the cavern. Upon completion of the ongoing benching operations, the measured performance from the walls of the cavern will be available for comparison with the existing numerical results. Permanent rock support in the cavern consists of systematic bolting of alternating lengths and mesh reinforced shotcrete S(mr). However, rock support design recommendations based on the Norwegian Method of Tunnelling (NMT), which employs wet process fibre reinforced shotcrete S(fr) instead of S(mr), have been numerically tested and verified. Copyright © 1996 Elsevier Science Ltd

INTRODUCTION

Rock mass classifications, which form the backbone of the empirical approach, have proven to be useful in providing guidelines for assessing the behaviour of rock masses and in choosing support requirements. Over 1050 cases have been analysed in the updating of the Q-system [1].

Ever since its development, the Q-system of Barton *et al.* [2], has attracted the attention of tunnel engineers, field geologists and researchers in its application to hard, jointed and faulted rocks. Construction engineers and geologists have preferred the empirical approach over the analytical and numerical approach, mainly because

of its simplicity. While classification of rock masses will never be a substitute for experience in tunnelling, there is no doubt that an approach using one of the established classification schemes, together with a suitable numerical modelling technique, can help in forecasting and in better understanding the behaviour of the ground.

With the advent of a new statistical method of logging the Q-system parameters and the more detailed joint and rock mass descriptors (JRC, JCS and ϕ_r), the empirical and numerical approaches have recently been suitably integrated [3,4]. The mapped geotechnical data together with the Q-system parameters can be conveniently incorporated into numerical models for predicting the behaviour of the rock mass and for validating the empirically derived reinforcement. The interaction between the potentially relevant variables for engineering design, such as rock type, discontinuities, stress,

†Norwegian Geotechnical Institute (NGI), Oslo, Norway.

‡National Institute of Rock Mechanics (NIRM), Bangalore, India.

Table 1. Summary of geotechnical data

Symbol	Definition	Set	Typical range	Mean/wt Average
W	Weathering		I-II	I
RQD	Rock quality designation		50-80	69.5
J_n	Joint set number		3-6	5.2
J_r	Joint roughness number	1	2-3	2.6
J_a	Joint alteration number	1	1-3	2.6
J_w	Joint water reduction factor		0.66-1.0	0.96
SRF	Stress reduction factor		2.5-5.0	4.9
Q			0.73-32.0	2.7
S	Joint spacing (m)	1	0.1-0.2	0.19
L	Joint length (m)	1	5-10	7.22
F	Joint frequency per metre		2-10	5.6
J_v	Joints per m ²		3-10	8.7
α, β	Joint direction (right hand rule) (°)	1	EW/30-50 N	EW/40 N
JRC	Joint roughness coefficient	1	2-8	5.7
a	Roughness amplitude per unit length ($L = 0.1$ m) (mm)	1	1-2	1.18
a	Roughness amplitude per unit length ($L = 0.5$ m) (mm)	1	5-10	7.64
ϕ_r	Residual friction angle (°)		22-26	24.5
JCS	Joint wall strength (MPa)		25-50	37.85
σ_c	Uniaxial compressive strength (MPa)		20-50	35
σ_1	Major principal stress (MPa)		5-10	7.14
K	Permeability (m/sec)		10^{-7} - 10^{-9}	10^{-8}

anisotropy, etc. has recently been explained through an interaction matrix in Rock Engineering Systems [5].

Besides providing general tunnel reinforcement recommendations, the Q-system has found widespread use with regards to estimating tunnel support pressures in loosening ground conditions [6], in estimating the Hoek-Brown [7] failure criterion parameters m and s [8], and in estimating *in situ* deformation modulus [9, 10]. The Q-system has also recently been used for the closer prediction of stress-strength related problems in tunnels [11].

In a comprehensive review and evaluation of the four most frequently used classification systems (RQD, RSR, RMR and Q) in four single railway tunnels in the Canadian Rocky Mountains, Kaiser *et al.* [12], concluded that the Q-system best predicted the required

tunnel support and that the selection of most parameter ratings in the Q-system was relatively straightforward because of the detailed guidance given in the rating tables. However, since variations in Q-values of more than one order of magnitude can result from the assessment of the stress reduction factor (SRF) alone, it is apparent that this parameter in particular should be carefully assessed based on the *in situ* stress to compression strength ratios of the rock mass.

In this paper, the distinct element method using the UDEC-BB code [13] and the updated empirical approach [1] have been applied for predicting the behaviour of the rock mass around a large excavation currently under construction in India. These predictive studies have been compared with the observations inside the cavern. The Q-system based design recommendation for use of fibre-reinforced shotcrete, as part of permanent reinforcement, has also been numerically tested and verified.

DETAILS OF INVESTIGATIVE STUDIES

A detailed engineering geological assessment of relatively low strength (< 50 MPa) metamorphosed rocks (schists) has been carried out at the site of an ongoing hydroelectric project in the Himalayan Region of India. Since the project involves the construction of a large number of quite large underground structures including a 10.5 m dia. and 27.3 km long head race tunnel, four desilting chambers (each 525 × 16.31 × 27.5 m) and a powerhouse (216 × 20 × 49 m), there was clearly a need to make a general assessment of the behaviour of such rocks when excavated on a large scale. The Central Water Commission (CWC), and the Central Soil & Materials Research Station (CSMRS), New Delhi, along with the Geological Survey of India (GSI), Nathpa Jhakri Power Corporation (NJPC), National Institute of Rock Mechanics (NIRM) and the

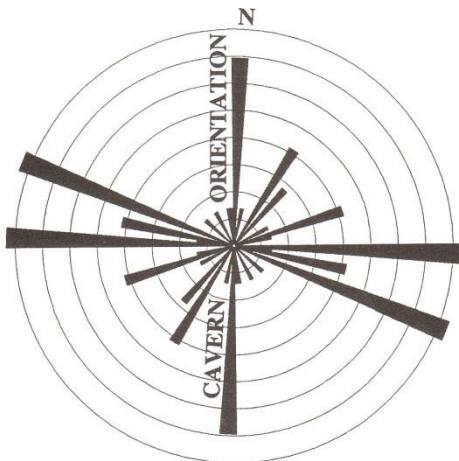


Fig. 1. Rose diagram showing the cavern and joint orientations.

Norwegian Geotechnical Institute (NGI) have been involved in performing predictive studies and performance monitoring of the powerhouse cavern. Emphasis was placed on the powerhouse area due to the large size of the cavity.

Table 1 gives a summary of the geotechnical data gathered from the powerhouse site. The area encompassing the powerhouse site contains essentially quartz-mica schist, patches of biotite schist and muscovite (sericite) schist. These are moderately to closely jointed rocks and at places slightly to moderately weathered [14]. During the exploratory and initial stages of cavern construction, detailed engineering geological mapping of the rock and rock joints had been carried out. The geological investigations involved detailed joint surveys of the surface exposures and the excavated portions of the powerhouse cavern (pilot tunnel and drift), providing data on joint orientations, conditions and spacing. Measurements of strike and dip of the main discontinuities were made throughout the survey. More than five joint sets have been recorded in the project area, but rarely more than three or three sets plus random are encountered at any one location. The East–West striking foliation joints, with 35° dip in the northerly direction, constitute the major discontinuities, while the other two sets of joints have a strike approx. in the NS direction (parallel to the cavern axis) and dip steeply ($70\text{--}90^\circ$) in the East and West directions, respectively. In places gouge seams are associated with

some of the joints, especially the foliation joints. In order to avoid wall stability problems, the alignment of the powerhouse cavity (N–S) was selected taking into consideration the strike direction (E–W) of the major discontinuity planes (Fig. 1).

Various experimental studies were conducted for finding the mineral assemblage, and the physical and mechanical properties of the rock masses. The rock mass classification approach using the Q-system was applied for estimating the support pressure and for evaluation of cavern reinforcement needs. A comprehensive engineering geological assessment of the rocks is given by Bhasin *et al.* [15], and a summary of the geotechnical data is presented in Table 1.

NUMERICAL MODELLING (PREDICTIVE) STUDIES

In jointed rock masses, a large part of the deformability may depend upon the rock discontinuities, such as joints, fractures, shear zones, etc. Having stated the above, it seems logical to employ a discontinuum approach to predict the jointed rock mass behaviour. The development of discontinuum modelling procedures such as the distinct element code [13], represents an important progress in modelling and understanding the mechanical deformation behaviour of jointed rock masses. The Universal Distinct Element Code (UDEC), containing the Barton–Bandis (BB) non linear joint behaviour model [16] has been developed for numerical

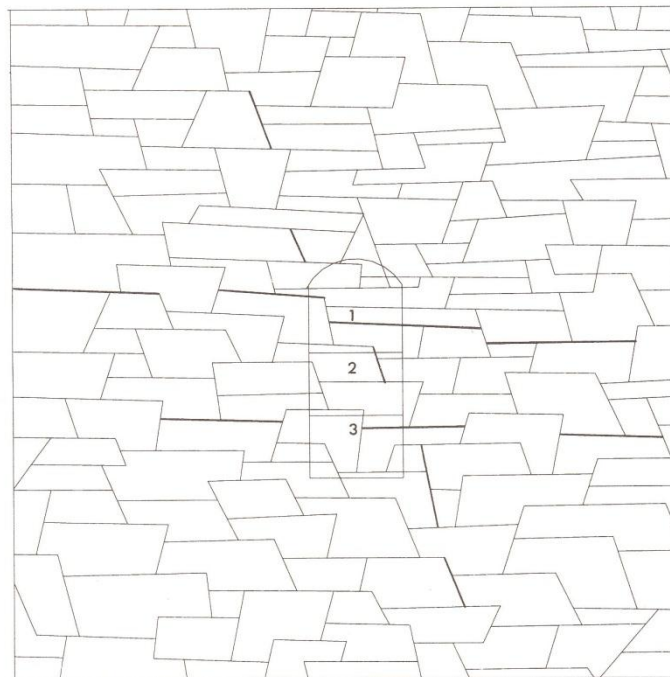


Fig. 2. Idealised joint model of the powerhouse cavern (see text for explanation).

simulation of underground structures in blocky ground in which the mechanical discontinuities play an important role in the overall deformation behaviour.

In general, the criterion for selecting the numerical modelling technique should consider at least two factors: the ground conditions (which may be represented by an established rock mass classification scheme), and the size of the excavation opening relative to the discontinuity type and spacing. For the case of the powerhouse cavern, three sets of joints had been identified and the ground conditions were logged using the Q-system and the data statistically recorded in geotechnical logging charts (see Table 1 for summary of geotechnical data).

Figure 2 shows the joint model containing the powerhouse cavern. This simplified and idealised model was constructed based on joint mapping performed at the surface and from the excavated (pilot tunnel) portion of the cavern. Three sets of joints and some discontinuities with gouge fillings (thick lines in figure) are represented in the model. The number of joints in the model is reduced compared to reality, and the easterly and westerly dipping joints are excessively long for all but the most persistent joints. The numbers within the cavern refer to the excavation steps. An inevitable approximation of 2D modelling is that joints perpendicular to the tunnel axis cannot be represented by the dip, while the joints trending parallel to the tunnel axis are representable with dip. The potential shortcomings and the source of errors due to exclusion of sub-perpendicular joints are difficult to estimate. However, the presence of additional sets non-parallel with the excavation tends to increase the deformation in practice, thus making a 2D approximation less conservative than usually assumed.

INPUT DATA FOR NUMERICAL MODELLING

The input data for the numerical modelling studies have been derived from field investigations, rock joint characterisation of drill core and from large scale joint roughness measurements, hydraulic fracturing stress measurements, and from Q-system logging (see Table 1 and ref. [15]). The Barton–Bandis [16] joint shear strength parameters (JRC, JCS and ϕ_r), used for predicting jointed rock mass behaviour, have been derived from joint roughness profiles, Schmidt hammer tests and tilt tests. Figure 3 shows, in the form of histograms and cumulative percent curves, the estimates of the three key shear strength parameters for input into the numerical analyses. The original form of the equation for the shear

strength of rock joints [17] is written as:

$$\tau = \sigma_n \tan \left[\text{JRC} \log \left(\frac{\text{JCS}}{\sigma_n} \right) + \Phi_r \right]. \quad (1)$$

Input parameters for the Barton–Bandis joint behaviour model were as follows:

$$\begin{aligned} \text{JRC}_0 &= 10 & \sigma_c &= 35 \text{ MPa} & L_n &= 1.0 \text{ m} \\ \text{JCS}_0 &= 37.85 \text{ MPa} & \phi_r &= 25^\circ \end{aligned}$$

where the subscripts (0) and (n) refer to lab scale (100 mm) and *in situ* block sizes (L_n), respectively (see ref. [18]).

The scale correction for *in situ* block sizes (L_n) is derived using the following scale correction equations [19]:

$$\text{JRC}_n = \text{JRC}_0 \left[\frac{L_n}{L_0} \right]^{-0.02\text{JRC}_0} \quad (2)$$

$$\text{JCS}_n = \text{JCS}_0 \left[\frac{L_n}{L_0} \right]^{-0.03\text{JRC}_0} \quad (3)$$

The residual friction angle ϕ_r is determined from Schmidt hammer and tilt tests using the following equation [17]:

$$\Phi_r = (\Phi_0 - 20^\circ) + 20 \left(\frac{r}{R} \right). \quad (4)$$

The shear strength of the discontinuities with gouge (alteration products) is estimated from the following Q-system relation:

$$\Phi_r = \tan^{-1} \left[\frac{J_r}{J_a} \right]. \quad (5)$$

Equation 5 represents a fair approximation to the shear strength that one might expect of the various combinations of wall roughness and alteration products [2]. The rock mass deformation modulus E is estimated from the following relation [9]:

$$E_{\text{mean}} = 25 \log_{10} Q = 10.78 \text{ GPa} \quad (6)$$

where $Q = 2.7$.

This relation gives good agreement with measured deformations when used in numerical analysis of tunnels and caverns at moderate depth (see, for example ref. [4]).

NUMERICAL RESULTS—PREDICTIONS

The results for each of the three excavated steps of the powerhouse cavern are summarised in Table 2. Figure 4 shows the displacement contours which give an indication of the excavation disturbed zone. A maximum of

Table 2. Summary of powerhouse cavern modelling results

Parameter	Step 1	Step 2	Step 3
Maximum principal stress (MPa)	19.1	24.1	24.6
Maximum displacement (mm)	17.7 (arch)	29.8 (wall)	45.2 (wall)
Maximum axial force on bolts (tons) without S(fr)	22.5	27.0	27.3
Maximum axial force on bolts (tons) with S(fr)	2.5	25.0	27.3

S(fr) = Shotcrete, fibre reinforced.

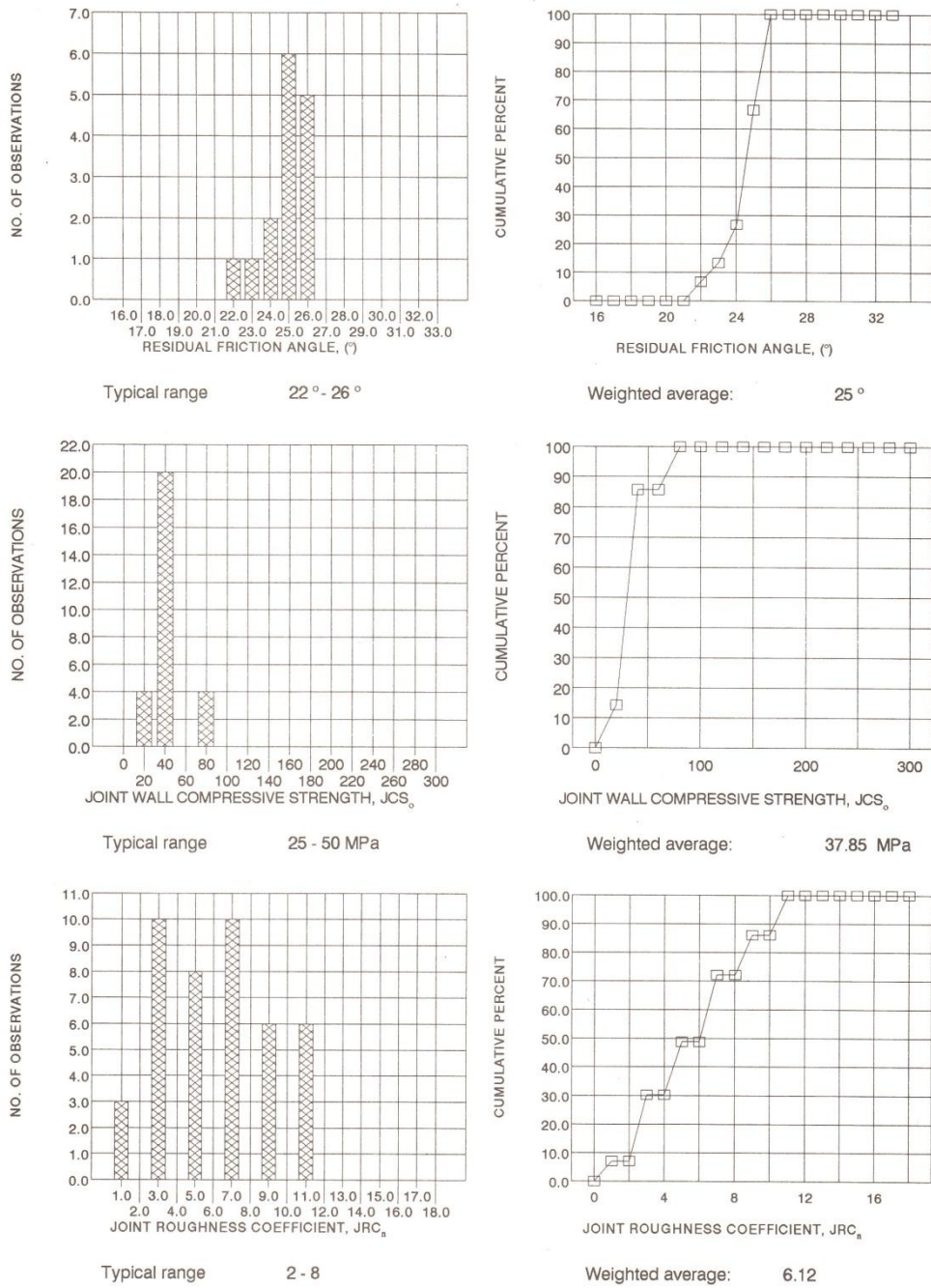


Fig. 3. Joint characterisation data showing the estimates of three key shear strength parameters.

45 mm of horizontal (x) displacement is predicted in the walls of the cavern after the excavation of the whole powerhouse cavern [see dotted black ornament on left wall in Fig. 4(c)]. Based on vertical (y) displacement contours after the first excavation step, it can be seen [Fig. 4(a)] that the shape of the excavation disturbed zone above the roof of the cavern is approximately symmetrical.

Figures 5 and 6 show bar graphs (from UDEC-BB output files) of the maximum principal stresses and displacements in the excavation disturbed zone as a function of the distance from the opening. It may be noted that, upon completion of the first excavation step [Fig. 5(a)–(c) step 1], relatively high tangential stresses (8–12 MPa), in relation to the unconfined compressive strength of the rock (<50 MPa), are developed in the proximity of the opening. This indicates potential for moderate spalling of rock material which in practice will be secured by reinforced shotcrete and systematic rock bolting. Although the phenomena of spalling is more common and can be severe in brittle rock types, non brittle rocks have also been observed to spall [20]. The spalling phenomena has been observed in sandstones, siltstones, shales and in this case schists [21]. Figure 6(a) (step 1) shows the predicted maximum displacement of 18 mm in the roof of the cavern, while Fig. 6(b) [step 3] shows the maximum displacement of 45 mm in the left wall of the cavern.

The development of bolt loads for 32 mm dia., 6 and 12 m long bolts placed alternatively at 3 m c/c spacing is shown in Fig. 7.

The reinforcement in the numerical model was designed to simulate actual practice where some permanent deformation (approx. 50% of total deformation) would have already occurred at the face in each of the excavated steps before the installation of bolts. Note the increases of bolt loading caused by the benching of the cavern. The maximum axial force on the bolts has increased from 22.5 tons at the end of excavation step 1 to 27.3 tons at the end of excavation step 3 (see Fig. 7 and Table 2).

PERFORMANCE MONITORING AND COMPARISON WITH NUMERICAL RESULTS

The construction of the powerhouse was started with a $7 \times 7 \times 216$ m long pilot tunnel which was completed in late 1994. A total of eight multi point borehole extensometers (MPBX, p1–p8) up to 20 m in length was initially installed in the roof of the pilot tunnel for monitoring of deformation. Upon completion of the pilot tunnel, four distinct sections along the tunnel length were identified so that eight more MPBX (w1–w8), four on each side of the upstream (left) and downstream (right) walls, could be installed. Figure 8 shows the locations of the MPBX in the widened and central portions of the pilot tunnel. The instruments in the widened portion were installed about 4 m (horizontal distance) from the upstream and downstream wall edges. The cross-sections in Fig. 8 show the anchor lengths (m)

and displacements (mm) near the centre of the cavern.

The instruments have been monitored regularly and at the time of writing this article (170 days after installation) a maximum of 24 mm deformation has taken place near the centre of the powerhouse cavern. The benching operations are progressing and the displacements in the roof have stabilised.

Figure 9 shows a plot of the maximum displacements recorded near the centre of the cavern. These results are quite similar to the numerical modelling results where approx. 18 mm of deformation had been predicted upon excavating the arch. The range of displacements recorded by the MPBX and the corresponding Q-values mapped in the cavern (see Fig. 8) provides data for comparison with Q-system case records [1]. Figure 10 shows an updated plot of the data measured during the excavation stages for Q/SPAN (in m) vs measured deformation (mm). All the recorded data points lie within the range of existing Q/SPAN-deformation trends. Although some more rock mass parameters, such as porosity and deformation modulus, can be incorporated in Fig. 10 for further refinement, the existing simplified relation provides a reasonable range of deformation values for a given rock mass quality and span of opening. As the benching operation progresses, 30 m long MPBX with remote controlled readouts are planned to be installed in the walls of the cavern for monitoring of displacements. The measured performance of the walls of the cavern may then be compared with the existing numerical results.

MODELLING OF FIBRE REINFORCED SHOTCRETE

The precise mechanism by which shotcrete acts in supporting an excavation is not well understood. Consequently, the majority of support designs are based on either monitoring during construction or from past experience using empirical guidelines such as those recommended by the Q-system. The primary objective of any support system is to help the rock mass support itself. Shotcrete helps in accomplishing this objective by preventing the rock mass from ravelling and loosening between the bolts, thereby allowing it to maintain its inherent load carrying capacity. Field observations indicate that shotcrete preserves the fabric of the rock mass allowing the arching action to develop fully, thereby restricting the kinematic freedom of blocks of rock.

The primary difference between plain reinforced shotcrete and steel fibre reinforced shotcrete S(fr) is that the unreinforced shotcrete is a relatively brittle material with little capacity to resist tensile stress without cracking, whereas the fibre reinforced shotcrete behaves in a ductile manner and offers considerable post peak strength [22, 23]. S(fr) also shows superior performance to single layer mesh reinforced shotcrete [24]. The wires of the mesh act as an obstacle for the shotcrete to reach the rock and may cause a shadow effect and a higher rebound. This affects the bond between the shotcrete layer resulting in poorer quality shotcrete behind the wires and the possibility of accelerated



Fig. 4. Displacement contours (m) between the three excavated steps. Max. disp. = 45 mm.

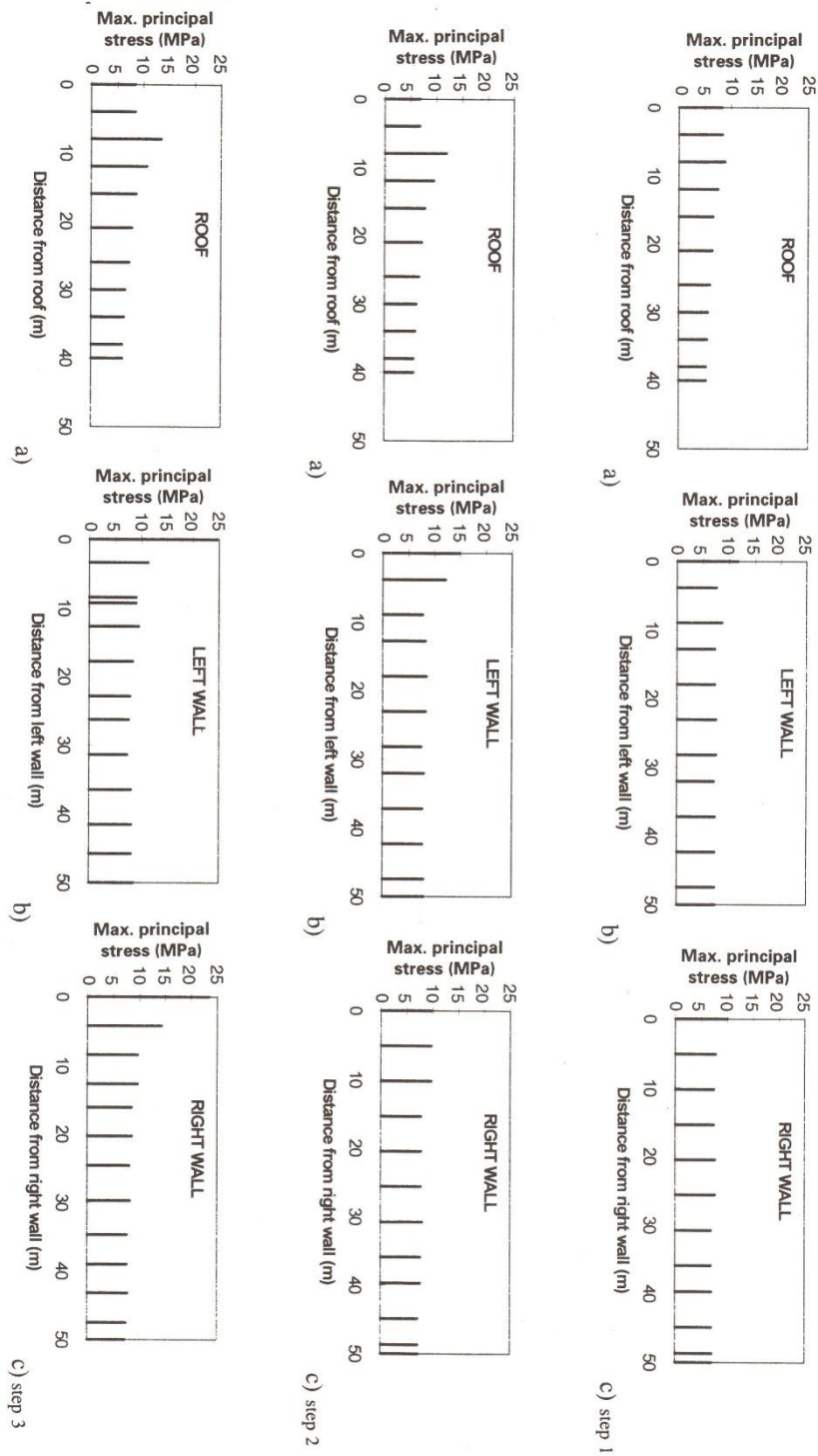


Fig. 5. Excavation disturbed zone analysis of principal stresses in the three excavation steps.

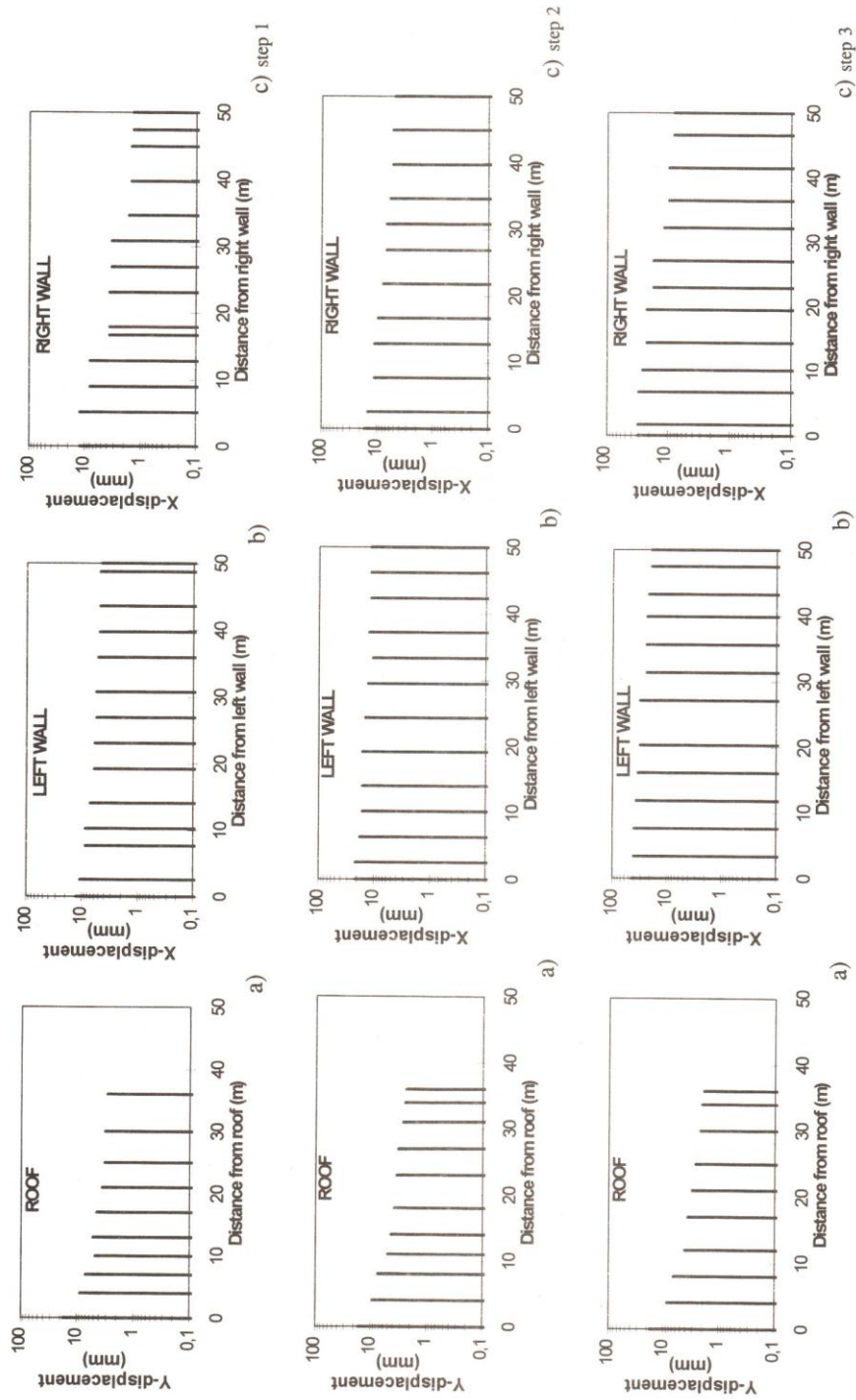


Fig. 6. Excavation disturbed zone analysis of displacements in the three excavation steps.

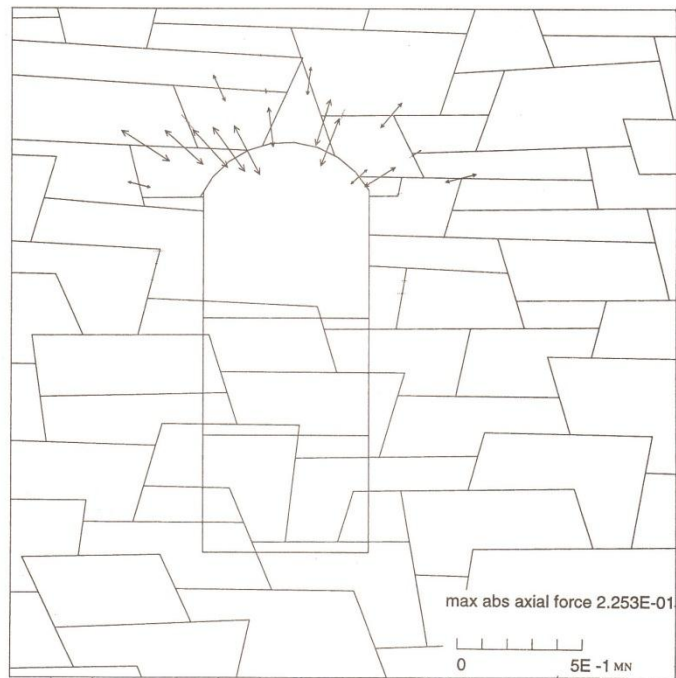


Fig. 7a

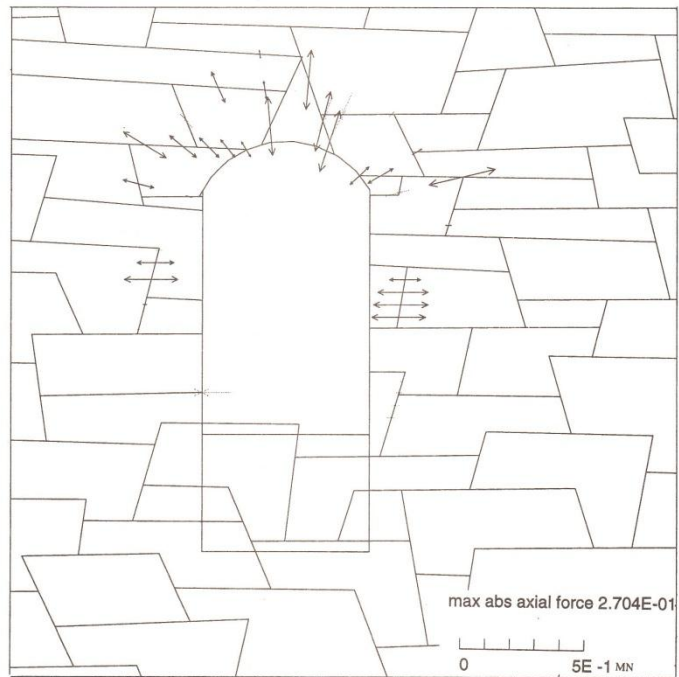


Fig. 7b

Figure 7 continued overleaf

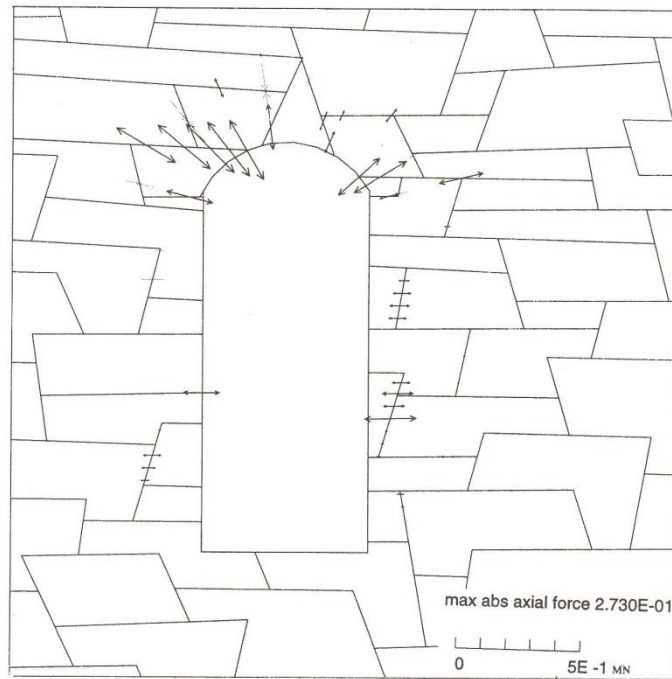


Fig. 7c

Fig. 7. Development of axial forces on rock bolts between the three excavated steps.

corrosion. In comparison, S(fr) can follow the exact contours of the rock and show a superior bond. When shotcrete is of good quality corrosion of the fibres is also inhibited.

In practice, if fibre reinforced shotcrete is to be used for reinforcement, a layer of shotcrete is immediately applied after a round has been blasted and the periphery scaled. The estimation of shotcrete thickness for initial support involves either the use of empirical rules or analytical models [25]. If analytical models are to be

used, then these should be correlated with empirical rules.

In the following, the Q-system based design recommendation for use of fibre reinforced shotcrete in the powerhouse cavern is numerically tested using the UDEC-S(fr) shotcrete modelling code [26]. In this code the analysis of the support structure (shotcrete) is initiated by discretisation of the structure into a number of elements (Fig. 11). The element's response to axial, transverse and flexural loads can be represented in the following matrix form:

$$\begin{bmatrix} T_1 \\ S_1 \\ M_1 \\ T_2 \\ S_2 \\ M_2 \end{bmatrix} = \frac{E}{L} \begin{bmatrix} A & & & & & \\ 0 & \frac{12I}{L^2} & & & & \\ & & SYM. & & & \\ 0 & \frac{6I}{L} & 4I & & & \\ -A & 0 & 0 & A & & \\ 0 & -\frac{12I}{L^2} & -\frac{6I}{L} & 0 & \frac{12I}{L^2} & \\ 0 & -\frac{6I}{L} & 2I & 0 & -\frac{6I}{L} & 4I \end{bmatrix} \begin{bmatrix} u_1 \\ v_1 \\ \theta_1 \\ u_2 \\ v_2 \\ \theta_2 \end{bmatrix} \quad (7)$$

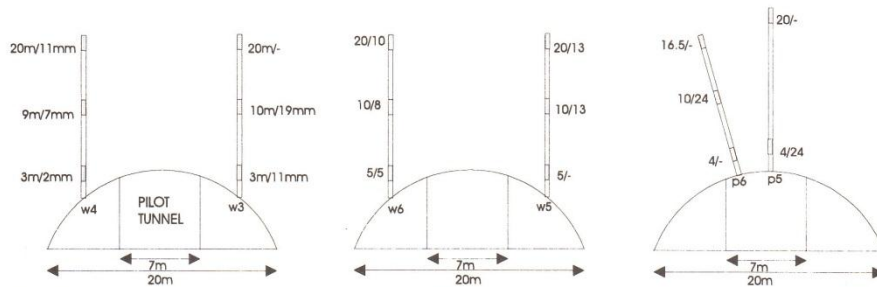
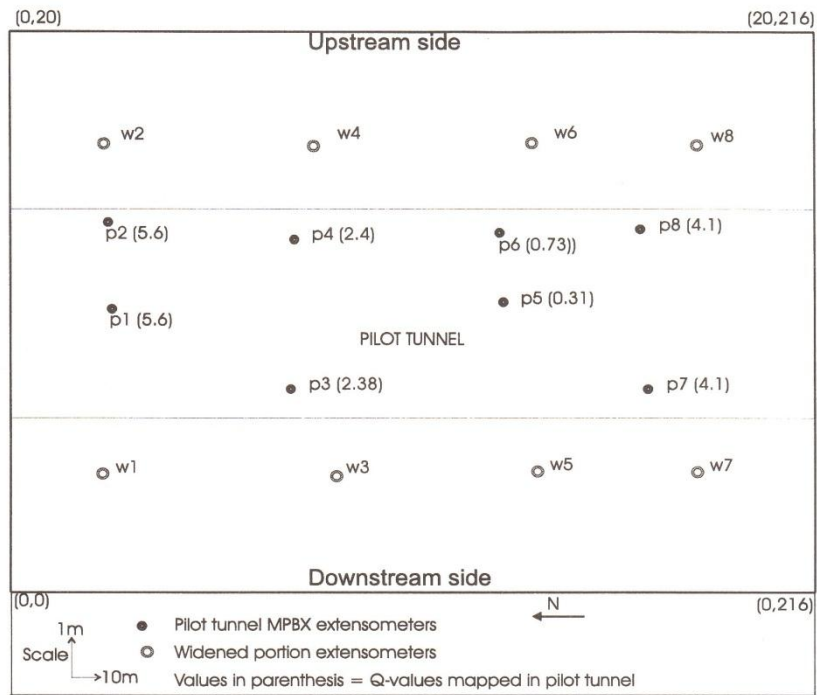


Fig. 8. Sketch of cavern showing the location of MPBX extensometers and cross-sections showing anchor length (m)/displacement (mm) near the centre of the cavern.

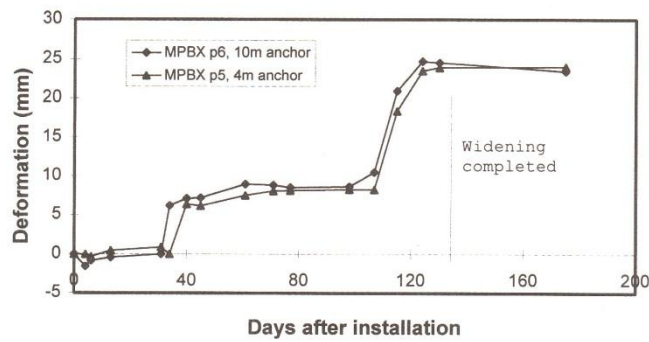


Fig. 9. Maximum displacements in the arch near the centre of the cavern.

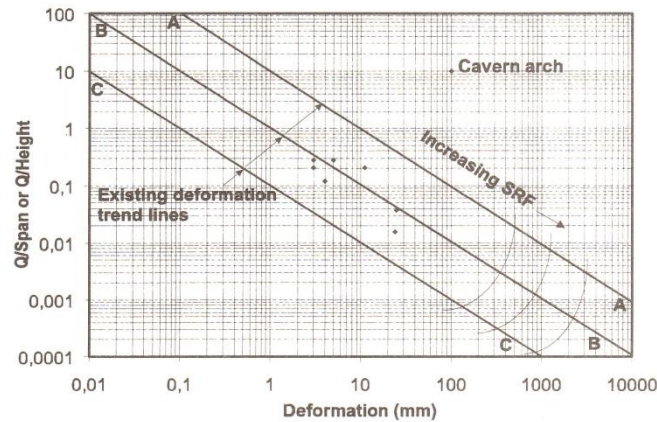


Fig. 10. Cavern arch displacements compared with Q-system data base.

In this formulation, T , S and M are the axial, transverse and flexural forces at the end points of an element and u , v and θ are the corresponding displacements. E , I , A and L are the modulus of elasticity, moment of inertia, area and length of the element.

The thickness of the structural element (10 cm thick shotcrete) has been derived from the support design chart contained in the updated Q-system. The engineering properties of the shotcrete, which included the compressive, residual, tensile and adhesive strength, were 30, 16, 2.75 and 0.5 MPa, respectively. Since the adhesive strength of shotcrete varies to a large extent with the rock type and mineralogy of the rock mass, an appropriate value of 0.5 MPa was chosen from the experimental results and theoretical studies carried out on the adhesion of shotcrete to various rock surfaces [27].

The application of shotcrete in the numerical model has been carried out in such a way to simulate actual conditions in practice where a layer of shotcrete is usually applied after a round is blasted and then rock bolts are installed. This allows proper integration of the support systems. The above routine was followed for each of the three excavated steps. The model in each of the excavated steps was allowed to run to equilibrium with modelled shotcrete before the installation of model rock bolts.

Figure 12 demonstrates the effect of the shotcrete on the bolt loading. This may be compared with the "bolt only" model shown in Fig. 7. Note the general reduction of bolt loads in the shotcrete model (see also Table 2). The supporting effect of shotcrete, after the first excavation step, can be seen on the right side of the shotcrete model, where some of the bolts show an axial compressive response (dotted lines). Upon further excavation (steps 2 and 3), the redistribution of stresses in the model causes the bolts to respond in axial tension. Clearly, there is generally a marked reduction in bolt loads (up to 10–20 tons) in the walls and in some areas

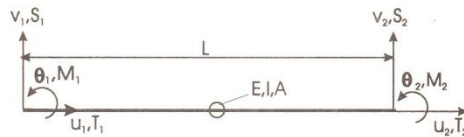


Fig. 11. Structural element showing the forces and displacements at end points (see text for explanation).

in the roof of the cavern in the shotcrete model, except for the stage 3 excavation.

Figure 13 shows the axial forces on the shotcrete. The effect of rock wedges is apparent. The maximum axial force on the structure is approximately 2.90 MN. This value is within the failure limit of 3 MN which is obtained by multiplying the compressive strength of shotcrete (30 MN/m^2) with the cross-sectional area [thickness (0.1 m) \times unit length (1 m) = 0.1 m^2] of shotcrete. The shear forces and bending moments (Fig. 14) are also within the limits of failure. The effectiveness of shotcrete at providing an initial support is obvious from the numerical results. By varying the thickness and engineering properties of shotcrete in the numerical model, rock support design charts incorporating partial factors of safety can be developed. These partial factor of safety support charts may then be used to compliment the existing empirical support design charts. In this way, the degree to which the support is oversized or undersized may be known. Work is being planned on these lines at NGI and is a subject of current research.

CONCLUSIONS

In this paper, updated empirical and numerical approaches have been applied to study the behaviour of the rock mass in a large underground cavern in the Himalayas. These predictive studies have been compared

In this formulation, T , S and M are the axial, transverse and flexural forces at the end points of an element and u , v and θ are the corresponding displacements. E , I , A and L are the modulus of elasticity, moment of inertia, area and length of the element.

The thickness of the structural element (10 cm thick shotcrete) has been derived from the support design chart contained in the updated Q-system. The engineering properties of the shotcrete, which included the compressive, residual, tensile and adhesive strength, were 30, 16, 2.75 and 0.5 MPa, respectively. Since the adhesive strength of shotcrete varies to a large extent with the rock type and mineralogy of the rock mass, an appropriate value of 0.5 MPa was chosen from the experimental results and theoretical studies carried out on the adhesion of shotcrete to various rock surfaces [27].

The application of shotcrete in the numerical model has been carried out in such a way to simulate actual conditions in practice where a layer of shotcrete is usually applied after a round is blasted and then rock bolts are installed. This allows proper integration of the support systems. The above routine was followed for each of the three excavated steps. The model in each of the excavated steps was allowed to run to equilibrium with modelled shotcrete before the installation of model rock bolts.

Figure 12 demonstrates the effect of the shotcrete on the bolt loading. This may be compared with the "bolt only" model shown in Fig. 7. Note the general reduction of bolt loads in the shotcrete model (see also Table 2). The supporting effect of shotcrete, after the first excavation step, can be seen on the right side of the shotcrete model, where some of the bolts show an axial compressive response (dotted lines). Upon further excavation (steps 2 and 3), the redistribution of stresses in the model causes the bolts to respond in axial tension. Clearly, there is generally a marked reduction in bolt loads (up to 10–20 tons) in the walls and in some areas in the roof of the cavern in the shotcrete model, except for the stage 3 excavation.

Figure 13 shows the axial forces on the shotcrete. The effect of rock wedges is apparent. The maximum axial force on the structure is approximately 2.90 MN. This value is within the failure limit of 3 MN which is obtained by multiplying the compressive strength of shotcrete (30 MN/m²) with the cross-sectional area [thickness (0.1 m) \times unit length (1 m) = 0.1 m²] of shotcrete. The shear forces and bending moments (Fig. 14) are also within the limits of failure. The effectiveness of shotcrete at providing an initial support is obvious from the numerical results. By varying the thickness and engineering properties of shotcrete in the numerical model, rock support design charts

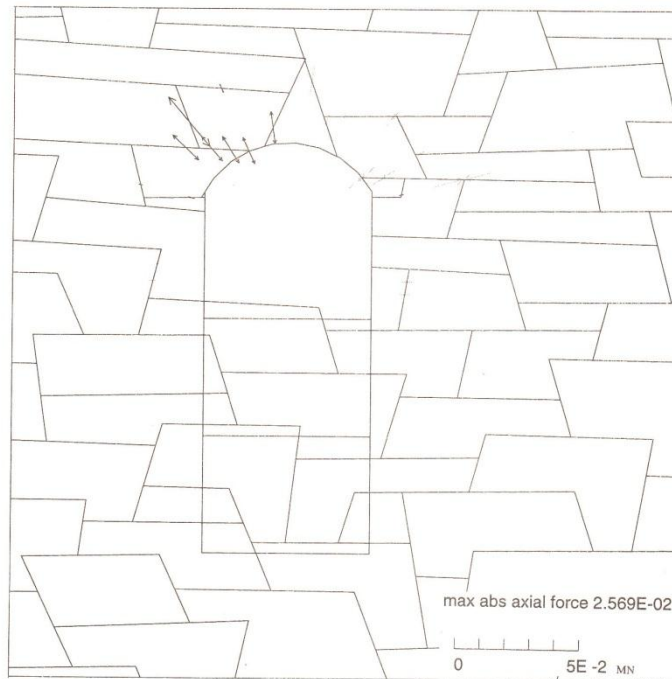


Fig. 12a

Figure 12 continued overleaf

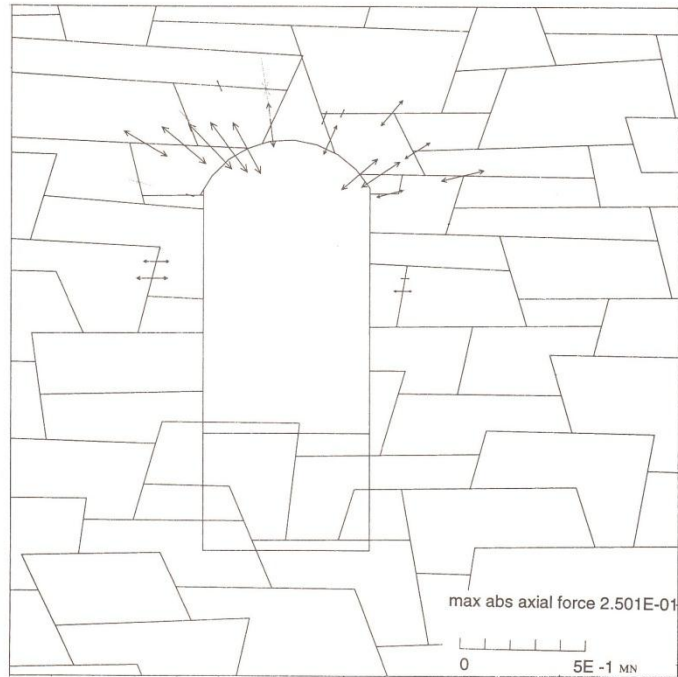


Fig. 12b

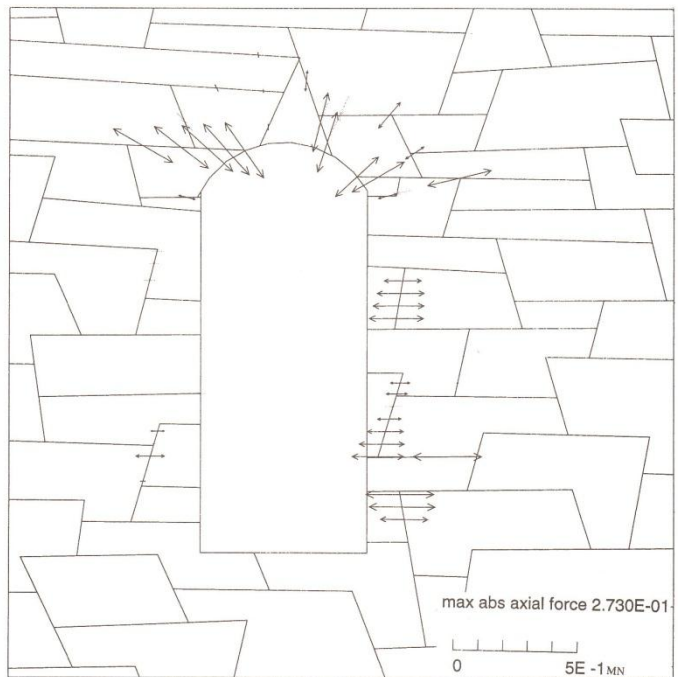


Fig. 12c

Fig. 12. Development of axial forces on rock bolts when SFRS is modelled.

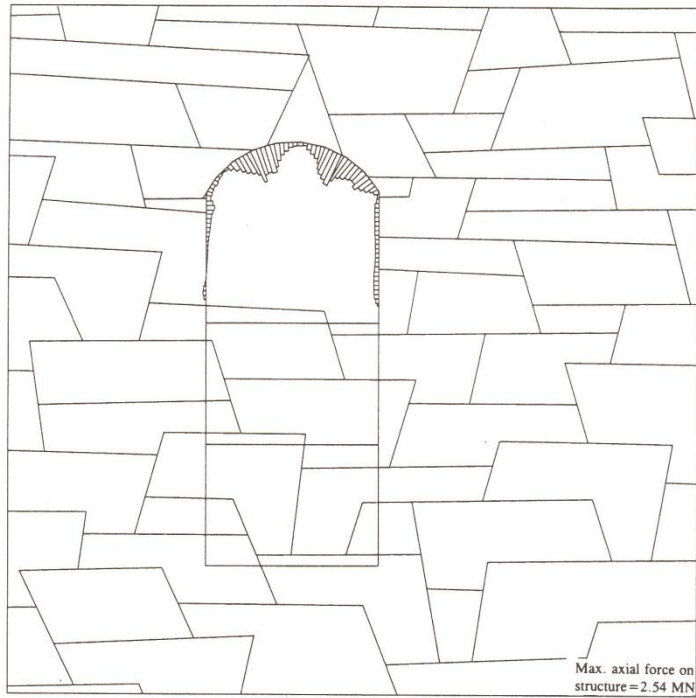


Fig. 13a

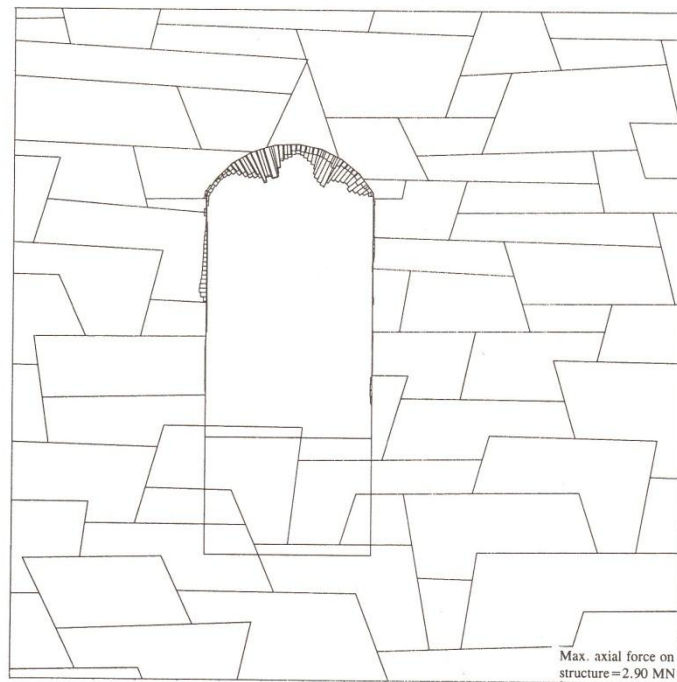


Fig. 13b

Figure 13 continued overleaf

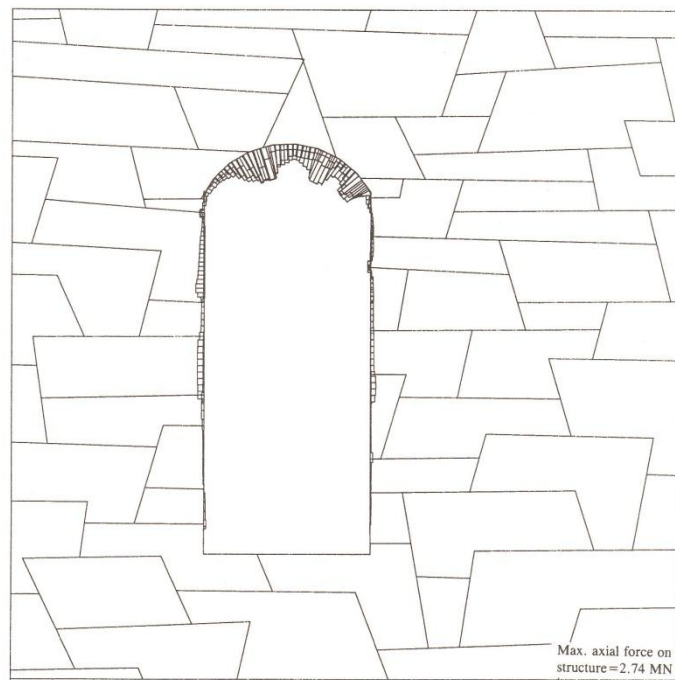


Fig. 13c

Fig. 13. Axial forces on the shotcrete. Max. axial force = 2.90 MN.

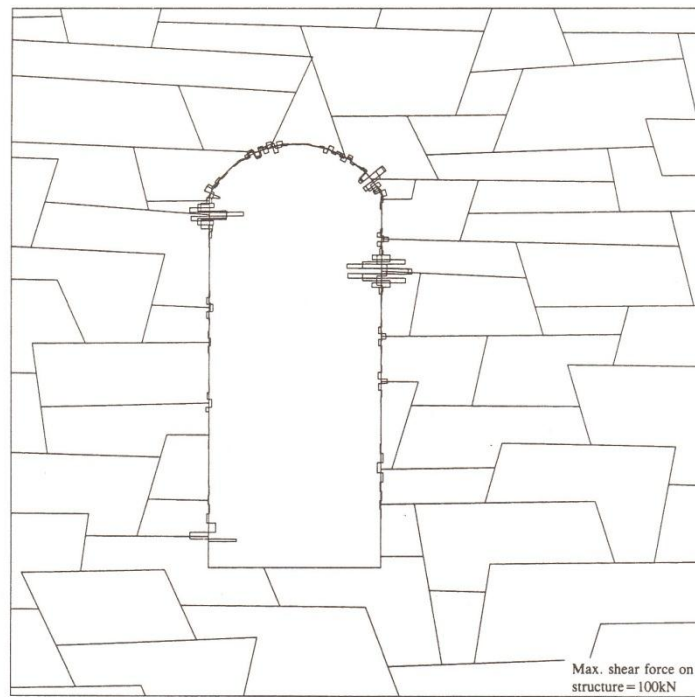


Fig. 14a

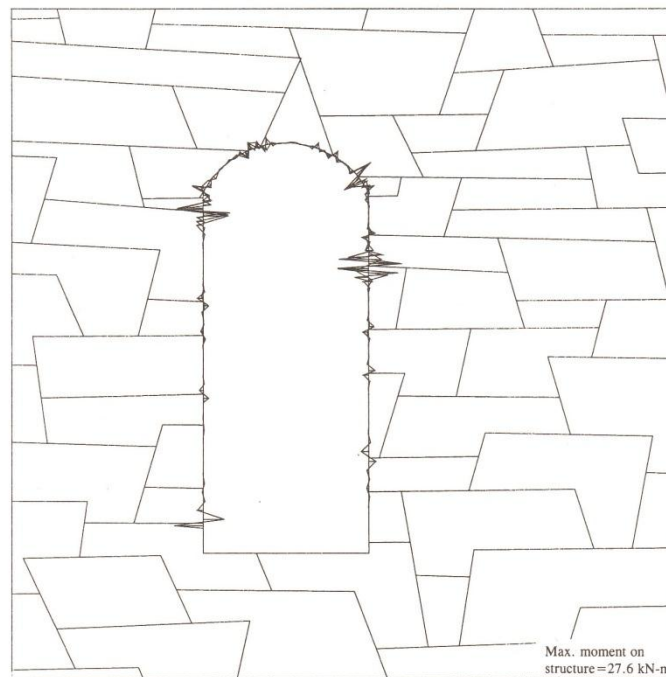


Fig. 14b

Fig. 14. Shear forces (kN) and bending moments (kN m) on the shotcrete.

with the instrumentation data from multi point borehole extensometers (MPBX). The results of deformation measurements indicate that the displacements in the periphery of the arch and in the deeper sections of the rock mass are similar to those predicted through the empirical and numerical approaches. The Q-system based design recommendation for use of fibre reinforced shotcrete as a part of permanent reinforcement in the powerhouse cavern is numerically tested using the UDEC-S(fr) modelling code. The effectiveness of shotcrete in providing an initial support is apparent and numerically demonstrated.

Acknowledgements—The authors would like to thank all the colleagues in NGL, CSMRS, NIRM, NJPC, GSI, CWC and JP Industries Ltd for their co-operation in assisting this research work. Professor Kaare Hoeg is thanked for his suggestions and review of the manuscript. The views expressed in the paper are those of the authors and not necessarily of the above mentioned organisations. The Norwegian Agency for Development (NORAD) is thanked for sponsoring the Indo-Norwegian CSMRS-NGL co-operation programme on tunnelling technology.

Accepted for publication 20 November 1995.

REFERENCES

- Grimstad E. and Barton N. Updating of the Q-system for NMT. *Proc. Int. Symp. Modern Use of Wet Mix Sprayed Concrete for Underground Support*, Fagernes 1993, pp.46-66, Norway (1993).
- Barton N., Lien R. and Lunde J. Engineering classification of rock masses for the design of tunnel support. *Rock Mech.* **6**, 189-236 (1974).
- Barton N., Løset F., Smallwood A., Vik G., Rawlings C. P., Chryssanthakis P., Hansteen H. and Ireland T. Geotechnical core characterisation for the U.K. radioactive waste repository design. *Proc. ISRM Symp. EUROCK*, Chester, U.K. (1992).
- Barton N., By T. L., Chryssanthakis P., Tunbridge L., Kristiansen J., Løset F., Bhasin R. K., Westerdahl H. and Vik G. Predicted and measured performance of the 62 m span Norwegian Olympic Ice Hockey Cavern at Gjøvik. *Int. J. Rock Mech. Min. Sci. & Geomech. Abstr.* **31**, 617-641 (1994).
- Hudson J. A. *Rock Engineering Systems: Theory and Practice*, pp.185. Horwood, Chichester (1992).
- Singh B., Jethwa J. C., Dube A. K. and Singh B. Correlation between observed support pressure and rock mass quality. *Tunnelling and Underground Space Technology* **7**, 59-74 (1992).
- Hoek E. and Brown E. T. Empirical strength criterion for rock masses. *J. Geotech. Engng Div., ASCE* **106**, 1013-1035 (1980).
- Hoek E., Kaiser P. K. and Bowden W. F. *Support of Underground Excavations in Hard Rock*, 215 pp. Balkema, Rotterdam (1995).
- Barton N. Application of Q-system and index tests to estimate shear strength and deformability of rock masses. *Proc. Int. Symp. Engineering Geology and Underground Construction*, Vol. 2:II.51-II.70, Lisboa (1983).
- Barton N. The influence of joint properties in modelling jointed rock masses, Keynote Lecture, ISRM Congress, Tokyo (1995).
- Bhasin R. K. and Grimstad E. The use of stress-strength relationships in the assessment of tunnel stability. *Tunnelling and Underground Space Technology* **11**, 93-98 (1996).
- Kaiser P. K., Mackay C. and Gale A. D. Evaluation of rock classifications at B.C. Rail Tumbler Ridge Tunnels. *Rock Mechanics and Rock Engineering* **19**, 205-234 (1986).
- Cundall P. A. A generalised distinct element program for modelling jointed rock. Report PCAR-1-80, Contract DAJA37-79-C-0548, European Research Office, U.S. Army, Peter Cundall Associates (1980).

14. ISRM. Rock characterisation testing and monitoring, Pergamon, England (1981).
15. Bhasin R. K., Barton N., Grimstad E. and Chryssanthakis P. Engineering geological characterisation of low strength anisotropic rocks in the Himalayan Region for assessment of tunnel support. *Engng Geology* 40, 169–193 (1995).
16. Barton N. and Bandis S. C. Review of predictive capabilities of JRC-JCS model in engineering practice. *Proc. Int. Symp. on Rock Joints*, pp. 603–610, Loen, Norway (1990).
17. Barton N. and Choubey V. The shear strength of rock joints in theory and practice. In *Rock Mechanics*, No. 1/2, pp. 1–54. Springer, Vienna (1977).
18. Makurat A., Barton N., Vik G., Chryssanthakis P. and Monsen K. Jointed rock mass modelling. *Proc. Int. Symp. on Rock Joints*, pp. 647–656. Loen, Norway (1990).
19. Barton N. and Bandis S. Effects of block size on the shear behaviour of jointed rock, Keynote Lecture, 23rd U.S. Symposium on Rock Mechanics, Berkeley, California (1982).
20. Ortlepp W. D. and Stacey T. R. Rockburst mechanisms in tunnels and shafts. *Tunnels and Underground Space Technology* 9, 59–65 (1994).
21. Grimstad E. and Barton N. Rock mass classification and the use of NMT in India. *Proc. Conf. on Design and Construction of Underground Structures*, 23–25 February 1995, pp. 63–74. New Delhi, India (1995).
22. Opsahl O. A. Steel fibre reinforced shotcrete for rock support. NTNF Project 1053.09511. Royal Norwegian Council for Scientific and Industrial Research (NTNF), Oslo, Norway (1982).
23. Vandewalle M. Tunnelling the World. N.V. Belkaert S.A., Bekaertstraat 2, 8550 Zwevegem, Belgium, pp. 218 (1991).
24. Holmgren B. J. Tunnel linings of steel fiber reinforced shotcrete. 5th International Congress on Rock Mechanics, Melbourne (1983).
25. Barrett S. V. L. and McCreath D. R. Shotcrete support design in blocky ground: Towards a deterministic approach. *Tunnelling and Underground Space Technology* 10, 79–89 (1985).
26. Lorig L. J. Modelling of fiber-reinforced shotcrete using UDEC-BB, draft manual, Itasca S.A. (1995).
27. Hahn T. and Holmgren J. Adhesion of shotcrete to various types of rock surfaces. *Proc. Int. Congress on Rock Mechanics*, pp. 431–439. Montreux (1979).